A comparison of three approaches for simulating fine-scale surface winds in support of wildland fire management. Part I. Model formulation and comparison against measurements

Jason M. Forthofer[A,B], *Bret W. Butler*[A] *and Natalie S. Wagenbrenner*[A]

[A]US Forest Service, Rocky Mountain Research Station, Missoula Fire Sciences Laboratory,
 5775 W Highway 10, Missoula, MT 59808-9361, USA.
[B]Corresponding author. Email: jaforthofer@fs.fed.us

Abstract. For this study three types of wind models have been defined for simulating surface wind flow in support of wildland fire management: (1) a uniform wind field (typically acquired from coarse-resolution (~4 km) weather service forecast models); (2) a newly developed mass-conserving model and (3) a newly developed mass and momentum-conserving model (referred to as the momentum-conserving model). The technical foundation for the two new modelling approaches is described, simulated surface wind fields are compared to field measurements, and the sensitivity of the new model types to mesh resolution and aspect ratio (second type only) is discussed. Both of the newly developed models assume neutral stability and are designed to be run by casual users on standard personal computers. Simulation times vary from a few seconds for the mass-conserving model to ~1 h for the momentum-conserving model using consumer-grade computers. Applications for this technology include use in real-time fire spread prediction models to support fire management activities, mapping local wind fields to identify areas of concern for firefighter safety and exploring best-case weather scenarios to achieve prescribed fire objectives. Both models performed best on the upwind side and top of terrain features and had reduced accuracy on the lee side. The momentum-conserving model performed better than the mass-conserving model on the lee side.

Introduction

Wind is one of the most influential environmental factors affecting wildland fire behaviour (Rothermel 1972; Albini 1982; Catchpole *et al.* 1998). Mechanical channelling and velocity variations induced by local terrain and vegetation can have a significant effect on the mean flow field, and can complicate fire behaviour prediction. Traditionally, fire managers have relied on expert judgment, point measurements or weather forecasts to estimate local winds (Rothermel 1993; Butler *et al.* 1998; USDA Forest Service and USDI Bureau of Land Management 2002); however, these methods can give large errors in complex terrain. A high-resolution wind model capable of simulating terrain-modified winds at sub-100-m scales could significantly benefit fire management.

When considering models that can be used as decision support tools for operational fire management, several constraints become evident: (1) minimum level of technical expertise required (i.e. extensive specialised training not required); (2) short decision-time-frame (i.e. less than 1 or 2 h); (3) minimum computing hardware (i.e. can be run on low-cost laptop computers) and (4) fine-scale spatial resolution (~100 m). These constraints preclude the application of traditional meteorological modelling methods that include a more complete set of sub-models describing the broad array of physical processes pertinent to atmospheric flow. The current project was organised with the explicit purpose of developing and testing models that meet these operational constraints.

Ideally, simulation of wildland fires should be linked to the atmosphere in a coupled fashion through latent and sensible heat fluxes (Linn *et al.* 2002; Clark *et al.* 2004; Mell *et al.* 2007; Sun *et al.* 2009). Sophisticated research tools, such as WRF-Fire (Coen *et al.* 2013) and WRF-SFire (Kochanski *et al.* 2013), have recently been developed to model coupled fire–atmosphere interactions and are likely to provide new information regarding the feedbacks of fire on atmospheric flows, and vice versa. However, these fully coupled models are not likely to be used in a truly operational sense anytime in the near future because of their high computational demands, coarse (~4 km) spatial resolution and the technical expertise required to run the models. In order to meet operational constraints, numerical fire spread models used for real-time incident support in wildfire management are typically operated in a decoupled mode (Finney 1998), such that there is no feedback between the fire and the atmosphere (USDA Forest Service and USDI Bureau of Land Management 2002; Stratton 2006; Ager *et al.* 2010; Finney *et al.* 2011).

Two general categories of wind models can be used to provide input to fire behaviour models: prognostic and diagnostic. Prognostic models – such as those used in numerical weather forecasting – solve conservation equations for mass, momentum, energy and moisture, and step forward in time. They commonly incorporate explicit schemes for boundary layer dynamics, land–atmosphere interactions, radiation, thermodynamics and cloud processes. Because of the added physical processes, prognostic model weather forecasts require significant computing resources, have complex initial and boundary conditions, and require highly trained specialists to run them (Homicz 2002). Such models typically employ horizontal grid resolutions of 4 km or larger and are generally limited in complex terrain by coordinate system constraints, to resolutions of greater than ~1 km (Lundquist *et al.* 2010). At these resolutions, the terrain-influenced flow effects relevant to fire spread prediction cannot be captured (Atkinson 1995; Kim *et al.* 2000).

Diagnostic or steady-state models predict the wind field at one instant in time. The result can be used to represent winds during a quasi-steady or time-averaged period. Diagnostic models apply conservation of mass, momentum, and energy singularly or fully to account for terrain effects on an initial flow field obtained from point measurements or a coarse-scale weather model. As there is no time stepping involved, diagnostic models usually have much lower computational requirements than prognostic models. Diagnostic models are commonly used for disaster response applications where fast computation times are required and the models are run by casual users with limited computing resources.

Diagnostic models fall into three categories according to the amount of physics incorporated. The first and simplest type is based solely on conservation of mass (Sherman 1978; Davis *et al.* 1984; Moussiopoulos and Flassak 1986; Geai 1987; Ross *et al.* 1988; Chan and Sugiyama 1997; Montero *et al.* 1998). Most of these models attempt to obtain a divergence free flow while minimising the change from an initial wind field. The more sophisticated mass-conserving models incorporate empirical parameterisations of phenomena such as non-neutral stability, kinematic effects and diurnal forcing (Scire *et al.* 2000).

The second type of diagnostic model solves a linearised momentum equation (Jackson and Hunt 1975; Mason and King 1985; Walmsley *et al.* 1986; Mortensen *et al.* 1993). A turbulence closure scheme is often included (Mellor and Yamada 1982). Computational times are similar to those of the mass-conserving models, but non-linear momentum effects in steep terrain are not represented (Lopes 2003). Dynamic linearised models and mass-conserving models have been found to give similar results (Walmsley *et al.* 1990; Barnard 1991; Finardi *et al.* 1993). Homicz (2002) concluded that mass-conserving models were better suited than linearised models for atmospheric dispersion of hazardous materials in emergency response scenarios.

The third type of diagnostic model considers conservation of mass and momentum with some form of turbulence closure (Raithby *et al.* 1987; Alm and Nygaard 1995; Apsley and Castro 1997; Maurizi *et al.* 1998; Uchida and Ohya 1999; Kim *et al.* 2000; Castro *et al.* 2003; Lopes 2003; Undheim *et al.* 2006) and sometimes conservation of energy (Montavon 1998). One of the major challenges with these types of models is solving the fluidised equations of motion under turbulent conditions.

Three general methods have been used to resolve turbulence: Reynolds averaging of the Navier–Stokes equations (RANS), large eddy simulation (LES) and direct numerical simulation (DNS) (Rodi 1997). Simulations using the RANS RNG k-ε turbulence model have been shown to handle non-linear flow effects, such as recirculation, better than mass-conserving models (Lopes 2003).

Diagnostic models are limited because of their inability to simulate evolution of the boundary layer due to transient and thermal effects. Prognostic models are limited by their requirements for significant technical expertise and computing resources. The coupling of wind flow models (such as the ones investigated in this study) to downscale coarse meso-scale numerical model outputs was first demonstrated in the late 1990s (Beaucage *et al.* 2014). Perhaps such a solution could be applied to support of wildland fire management.

Typically, wildland fire decision support systems have used wind data acquired from coarse-scale weather service models. Such data are used to construct a domain-average wind field (hereafter termed *uniform wind field*). The primary focus of this presentation is to describe two newly developed diagnostic models that have been formulated to bridge the gap between desired wind resolution for fire management and the capabilities of prognostic models (i.e. the source of uniform wind fields). The two new models correspond to the first and third types of diagnostic models described above: a mass-conserving approach (hereafter termed *mass conserving*) and a mass and momentum-conserving approach (hereafter termed *momentum conserving*). The overall goal of this research is to assess the capability of the two new models to provide wind predictions in complex terrain. The specific objectives of this work are to (1) describe the technical foundations of the mass-conserving and momentum-conserving models; (2) compare model-predicted surface wind speeds and directions to existing datasets collected during two field campaigns in complex terrain; and (3) investigate model sensitivity to mesh resolution and aspect ratio. Comprehensive evaluations of sensitivity of predicted winds to model input parameters, atmospheric stability (neutral stability is assumed here) and terrain type are left for future studies. A companion study compares the results of fire growth simulations based on the three wind model types (Forthofer *et al.* 2014).

Methods

Mass-conserving numerical model

Model description

The mass-conserving model seeks to minimise the change from an initial wind field while conserving mass (Sasaki 1958, 1970*a*, 1970*b*). The function to minimise is constructed using the square of the difference between the adjusted and initial winds:

$$E(u_1, u_2, u_3) = \int_{\Omega} \left[\alpha_1^2 (u_1 - \hat{u}_1)^2 + \alpha_1^2 (u_2 - \hat{u}_2)^2 + \alpha_2^2 (u_3 - \hat{u}_3)^2 \right] d\Omega$$

(1)

The computational domain is denoted by Ω, α_1 and α_2 are the Gauss precision moduli, u_1, u_2 and u_3 are the velocity components in the x_1 (positive to east), x_2 (positive to north), and x_3 (positive upward) directions. The initial values of velocity are $\hat{u}_1$, $\hat{u}_2$ and $\hat{u}_3$. The minimum value of $E(u_1, u_2, u_3)$ will give the minimal change from the initial velocity field in a least-squares sense. The Gauss precision moduli control the relative amount of change induced by the model in the horizontal and vertical directions. A value of 1 for both $\hat{u}$ moduli was used in this work, which creates a situation (numerically) in which the change in flow can occur equally in the horizontal and vertical directions, which is representative of neutral atmospheric conditions.

The minimisation of Eqn 1 is subject to the constraint that the resulting wind field must conserve mass:

$$H(u_1, u_2, u_3) = \frac{\partial u_i}{\partial x_i} = 0 \qquad (2)$$

where $i = 1, 2, 3$ and Einstein summation notation is used.

Using Lagrange multiplier theory, the problem becomes one of minimising the modified functional:

$$F(u_1, u_2, u_3, \lambda) = E(u_1, u_2, u_3) + \int_\Omega \lambda H(u_1, u_2, u_3) d\Omega$$

$$= \int_\Omega \left[\alpha_1^2(u_1 - \hat{u}_1)^2 + \alpha_1^2(u_2 - \hat{u}_2)^2 + \alpha_2^2(u_3 - \hat{u}_3)^2 + \lambda \frac{\partial u_i}{\partial x_i} \right] d\Omega$$

$$(3)$$

Here, $\lambda(x_1, x_2, x_3)$ is a Lagrange multiplier. The minimum of (3) is found from the solution of the associated Euler–Lagrange equations:

$$u_1 = \hat{u}_1 + \frac{1}{2\alpha_1^2} \frac{\partial \lambda}{\partial x_1}, \quad u_2 = \hat{u}_2 + \frac{1}{2\alpha_1^2} \frac{\partial \lambda}{\partial x_2},$$

$$u_3 = \hat{u}_3 + \frac{1}{2\alpha_2^2} \frac{\partial \lambda}{\partial x_3}, \quad \frac{\partial u_i}{\partial x_i} = 0 \qquad (4)$$

which are subject to the boundary condition:

$$\lambda \delta \vec{V} \cdot \vec{n} = 0 \text{ on } \Gamma \qquad (5)$$

where Γ is the bounding surface of the domain ($\vec{V} = (u_1, u_2, u_3)$), $\vec{n}$ is the outward unit vector normal to the bounding surface of the domain and $\delta \vec{V}$ is the first variation of the velocity.

The Euler–Lagrange equations (Eqn 4) are reduced to one equation by taking the partial derivatives of the first three equations (with respect to x_1, x_2 and x_3) and substituting into the last equation (Eqn 5). To simplify notation, let $\alpha^2 = \alpha_1^2/\alpha_2^2$ where $\alpha_1 = \alpha_2 = 1$. The result is an elliptic partial differential equation for λ:

$$\frac{\partial^2 \lambda}{\partial x_1^2} + \frac{\partial^2 \lambda}{\partial x_2^2} + \alpha^2 \frac{\partial^2 \lambda}{\partial x_3^2} = -2\left(\frac{\partial \hat{u}_i}{\partial x_i}\right) \qquad (6)$$

Once the $\lambda(x_1, x_2, x_3)$ field is found, the adjusted wind velocities are computed from Eqn 4. The boundary condition used on 'open' or 'flow-through' boundaries is $\lambda = 0$. This implies that the normal derivative in general is not zero, which gives a non-zero adjustment to the normal velocity (see Eqn 4). In the non-normal directions, the derivative is zero so no adjustment is made to those components of velocity. A Neumann condition is imposed at the ground boundary, that is, $(\partial \lambda)/(\partial \vec{n}) = 0$. This implies that the velocity normal to the ground surface is not adjusted from its initial value. As the velocity at the ground nodes is initialised to zero, the adjusted velocity is also zero thereby creating an 'impermeable' boundary.

The numerical solution to Eqn 6 is obtained using finite element techniques as described in, for example, Thompson (2005). The elliptic Poisson's equation for λ is written in a weak form and Galerkin's method is used. The resulting finite element equations form a system of coupled, linear, algebraic equations that are solved using a conjugate gradient method with Jacobi preconditioning (Barrett *et al.* 1994). The elliptic equation is solved on a terrain-following coordinate system consisting of layers of hexahedral cells that grow vertically with height.

Mass- and momentum-conserving numerical model
Model description

The momentum-conserving model uses the commercial computational fluid dynamics (CFD) code Fluent (see www.fluent.com, accessed 1 February 2006) to simulate wind flow over terrain. The fluid is considered to be steady, viscous, incompressible and turbulent. Geometry effects of the terrain are assumed to dominate the local flow field. The fluid density is constant at 1.225 kg m^{-3} so there is no buoyancy term in the vertical momentum equation and therefore the energy equation is not solved. Air temperature is set to 300K and the diagnostic models assume neutral stability. Coriolis effects are neglected. The Reynolds averaging procedure is applied to the Navier–Stokes equations and the resulting mass and momentum equations are:

$$\frac{\partial u_i}{\partial x_i} = 0 \qquad (7)$$

$$\frac{\partial(\rho u_i u_j)}{\partial x_j} = -\frac{\partial p}{\partial x_i} + \frac{\partial}{\partial x_j}\left[\mu\left(\frac{\partial u_i}{\partial x_j} + \frac{\partial u_j}{\partial x_i}\right)\right] + \frac{\partial}{\partial x_j}(-\rho \overline{u_i' u_j'}) \quad (8)$$

where $i, j = 1, 2, 3$, u_i and u_j, are the time-averaged velocity components in the i and j coordinate directions, u_i' and u_j' are the velocity perturbations in the i and j directions, p is pressure, ρ is density, μ is laminar viscosity and Einstein summation notation is used. The Reynolds stresses ($-\rho \overline{u_i' u_j'}$) are modelled using the Boussinesq hypothesis (Boussinesq 1877). Turbulence is modelled using the RNG $k - \varepsilon$ turbulence model (Yakhot and Orszag 1986).

The governing partial differential equations are discretised using the finite volume method to produce a set of coupled, linear equations. Second-order central differencing is used for all diffusion terms and a second-order upwind scheme is used for the advection terms. Pressure–velocity coupling is achieved using the SIMPLEC (Vandoormaal and Raithby 1984) algorithm. The equations are solved in a segregated way, using a point implicit solver (Gauss–Seidel) with an algebraic multi-grid method.

The discretised equations are solved on an unstructured, collocated numerical grid (Kim and Boysan 1999; Stangroom 2004). Two types of meshing schemes were used in this work: (1) a hexahedral mesh with vertical stretching of cells with height above the ground and (2) a hybrid mesh consisting of several layers of prismatic cells near the ground and tetrahedral cells above that grow in size with increasing height above the ground.

The boundary conditions at inlet surfaces are described by velocity boundary layer profiles that are a function of height above the ground. The functional forms used are similar to those recommended by Richards and Hoxey (1993):

$$U = \frac{u_*}{K} \ln\left(\frac{z}{z_0}\right) \tag{9}$$

$$k = \frac{u_*^2}{\sqrt{C_\mu}} \tag{10}$$

$$\varepsilon = \frac{u_*^3}{Kz} \tag{11}$$

where U is horizontal velocity, K is the Von Karman constant (0.41), z is height above the ground, z_0 is surface roughness length, k is the turbulent kinetic energy and C_μ is a constant equal to 0.0845. The friction velocity (u_*) is computed as:

$$u_* = \frac{KU_h}{\ln(\frac{h}{z_0})} \tag{12}$$

where U_h is the input wind velocity at some height above the ground h.

As the boundaries of the rectangular numerical grids used may or may not be parallel or perpendicular to the input wind direction, there can be one or two inlet boundaries. These inlet boundaries have a velocity magnitude equal to U in the appropriate direction. If the input direction aligns with the boundaries, there will be one inlet boundary, two side boundaries and one outlet boundary. If the input direction is oblique to the boundaries, two inlet boundaries and two outlet boundaries are used. Allowing wind directions not parallel or perpendicular to the boundary surfaces permits use of the same grid for multiple wind directions. Side and top boundaries use symmetry conditions where the normal velocity component is set to zero and the normal gradients of all other variables are set to zero. The boundary condition on outlet surfaces consists of setting the static (gauge) pressure to zero and the reference pressure to 101 325 Pa. In this Fluent solver, the hydrostatic pressure component is taken into the body force term, but because we are assuming constant density, it is zero. All other values are extrapolated from the interior of the domain.

A no-slip condition is specified at the ground boundary assuming the surface is aerodynamically rough by using a logarithmic relationship to bridge the gap between the surface and the inertial sub-layer. For micro-scale atmospheric simulations, the following relationship is normally used in the near wall cell:

$$U_p = \frac{u_*}{K} \ln\left(\frac{z_p}{z_0}\right) \tag{13}$$

Here, U_p is the velocity at the centre of cell p of the near wall cell and z_p is the distance from the ground to the cell centre. In Fluent, however, the following relationship is used for fully rough walls:

$$\frac{U_p C_\mu^{1/4} k^{1/2}}{\tau_w/\rho} = \frac{1}{K} \ln\left(\frac{Ez_p(\rho C_\mu^{1/4} k^{1/2})\mu^{-1}}{1 + C_s K_s(\rho C_\mu^{1/4} k^{1/2})\mu^{-1}}\right) \tag{14}$$

Here τ_w is the wall shear stress, E is an empirical constant (= 9.793), C_s is a roughness constant, and K_s is a roughness height. As $u_* = \sqrt{\tau_w/\rho}$ and in an equilibrium turbulent boundary layer $u_* = C_\mu^{1/4} k^{1/2}$, Eqn 14 can be rearranged to a form that resembles Eqn 13. To do this, the term $\mu(\rho C_\mu^{1/4} k^{1/2})^{-1}$ is assumed to be zero. The approximation is reasonable because this term is small compared to the other terms for atmospheric flows. The resulting equation is:

$$U_p = \frac{u_*}{K} \ln\left(\frac{Ez_p}{C_s K_s}\right) \tag{15}$$

So, if $C_s = E$ and $K_s = z_0$ and, then Eqns 13 and 15 are equivalent giving the usual atmospheric boundary layer wall condition.

The boundary condition for k at the wall is $(\partial k)/(\partial \vec{n}) = 0$ if n is the direction normal to the wall. The production of turbulent kinetic energy at the wall-adjacent cells (G_k) is computed assuming local equilibrium between turbulence production and dissipation. The production of k is computed as:

$$G_k = \tau_w \frac{\tau_w}{K\rho C_\mu^{1/4} k_p^{1/2} z_p} \tag{16}$$

and ε_p is computed from:

$$\varepsilon_p = \frac{C_\mu^{3/4} k_p^{3/2}}{Kz_p} \tag{17}$$

Note that the ε_p transport equation is not solved in the near wall cells, but directly computed from Eqn 17. Surface roughness length is constant over the entire domain. Additional information on the equations used can be found in 'Fluent User's Guide' (www.fluent.com).

As configured for this study, both models assume a neutrally stable atmosphere. This is a reasonable approximation for the high-wind conditions often associated with quickly spreading wildfires where there is sufficient mixing within the boundary layer, such that thermal effects (e.g. moisture transport, solar heating and cooling in the context of non-neutral stability) can be ignored (Byram and Nelson 1974; Parkinson 1987; Stangroom 2004). Additional model details can be found in Forthofer (2007).

Model evaluations with observed data

Few datasets exist in the literature for validating high-resolution wind models in complex terrain. The Askervein Hill data (Taylor and Teunissen 1983, 1985) were chosen because they constitute one of the only datasets reported in the archival literature at the spatial resolution relevant to fire management in

complex terrain. The Waterworks Hill data (Bradshaw 2004) were chosen as the second dataset for evaluations in this work because they represent wind flow over slightly more complex topography measured by a dense array of surface wind sensors for a location with essentially flat terrain upwind of the hill along the prevailing wind direction, and available upwind measurements of the approach flow at a permanent monitoring station. Surface wind speed and direction were chosen as the metrics for evaluation in this study because they are the primary data used by typical operational fire spread models (Rothermel 1972; Finney 1998).

A single flow event was selected from each observed dataset for model evaluation. Diagnostic models predict the spatial variability in the winds resulting from mechanical effects of the underlying terrain on the flow field. Thus, it is the reproducibility of the spatial variability in a given flow field at some snapshot in time that is of interest in this study. The specific wind events were chosen because they were periods with sustained strong wind speeds that are often associated with the most active fire behaviour.

Preliminary simulations identified some key model parameters that were examined in a sensitivity analysis. A more thorough sensitivity analysis was done for the mass-conserving model than the momentum-conserving model because the momentum-conserving model uses commercial code with well-established guidance on most parameters (www.fluent.com). The mass-conserving model was developed by the authors.

Askervein Hill: data description

Askervein Hill (57°11.313′N, 7°22.360′W) is 116 m high and is surrounded by flat terrain that averages 8 m above sea level with low vegetative cover. Measurements were collected 10 m above ground level from more than 50 measurement towers spaced nominally 100 m apart along three transects (Fig. 1). The reported 10-min average wind speed and direction data were averaged over 3 h to more closely match the modelling approaches followed in this study. The datasets used were identified as MF03-D and TU03B (Taylor and Teunissen 1985) and correspond to an average flow of 8.9 m s^{-1} from a direction of 210° at a reference site ~3 km upstream from the hill. The atmospheric stability was near neutral (average Richardson numbers of -0.0110–-0.0074). The ground roughness length was estimated at $z_0 = 0.03$ m (Taylor and Teunissen 1987). Elevation data consisted of 'Map B' in Walmsley and Taylor (1996) at 23-m horizontal spatial resolution and the domain size was ~6 km on a side.

Askervein Hill mass-conserving configuration. The computational mesh measured 6 km in both the north–south and east–west directions, with the hill located approximately in the centre. The top of the computational domain was 1000 m above sea level.

The simulation domain was initialised using information from the vertical velocity profile data measured at the upstream reference site. A power law Eqn 18 was used because it provided a better fit ($R^2 = 0.999$) to the data than the standard logarithmic profile ($R^2 = 0.984$) Eqn 9 (Fig. 2).
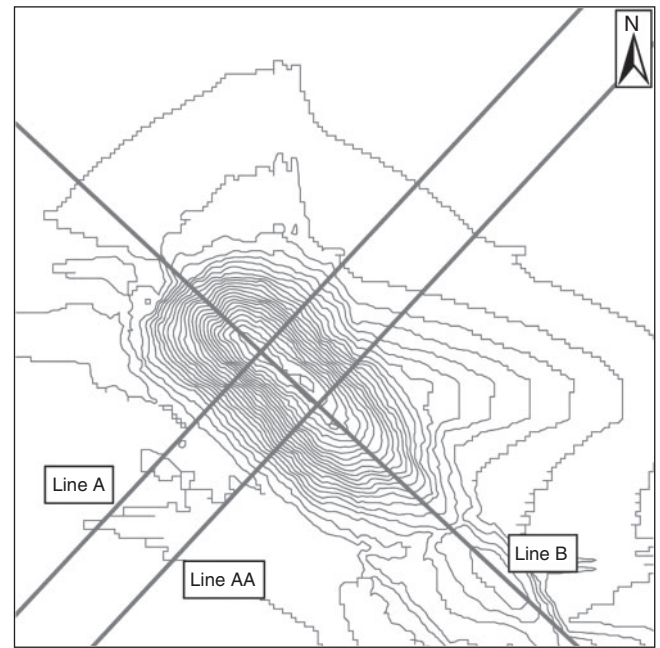
$$U = 5.3792z^{0.2113} \tag{18}$$

Fig. 1. Contour map of Askervein Hill showing locations of Lines A, AA and B. The elevation contour interval is 5 m.
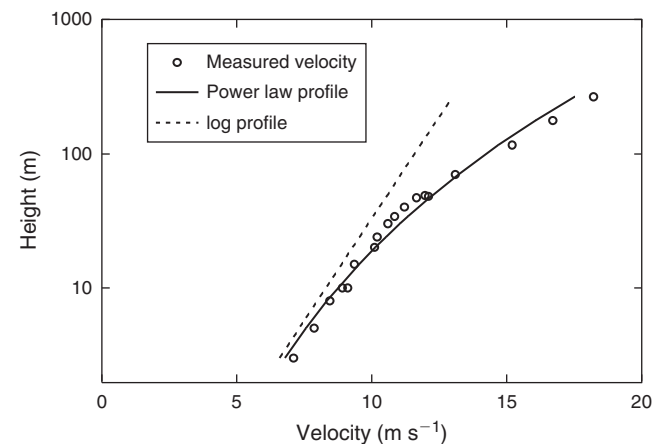

Fig. 2. Comparison of wind velocities with a logarithmic (Eqn 9) ($R^2 = 0.984$) and power law (Eqn 18) ($R^2 = 0.999$) equation at the upstream reference site at Askervein Hill on semi-log axes.

In this equation, U is the velocity and z is the height above the ground.

A base case simulation was done using the model parameters shown in Table 1. Additionally, several other simulations were done to show model sensitivity to some important model parameters (Table 2). These points are discussed in the following results.

Askervein Hill momentum-conserving configuration. Two grids of differing resolution were evaluated; each consisted of structured hexahedral cells in a terrain-following layered configuration with vertical stretching (Table 3). The near ground layer in both grids was 1 m tall.

**Table 1. Mass-conserving model base case parameters used for Askervein Hill simulations**

Residual tolerance	0.1
Number of quadrature points	1
Horizontal resolution (m)	40
Number of vertical cells	20, growth rate 30%
Cell aspect ratio	23

Table 2. Variations on mass-conserving model base case parameters for Askervein Hill simulations

Number of quadrature points	27 (at horizontal resolution of 120 m)
Horizontal resolution (m)	23, 60, 120
Number of vertical cells	15, 30, 35, growth rate 30%
Cell aspect ratio	590, 983

Table 3. Momentum-conserving model parameters used for Askervein Hill and Waterworks Hill simulations

Askervein Hill		Waterworks Hill	
Horizontal resolution (m)	Total cells	Horizontal resolution (m)	Total cells
40	500 000	80	842 000
23	2 000 000	23	1 529 000
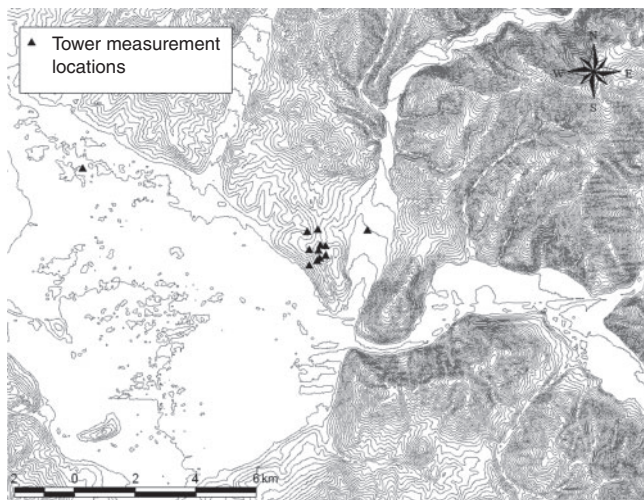
Fig. 3. Topographic map of Waterworks Hill and surrounding area. The west-most tower is the Missoula Airport tower and the east-most tower is the Tulip Tower. The other 10 towers are located on the actual hill. The elevation contour interval is 20 m.

Waterworks Hill: data description

Wind speeds were measured on Waterworks Hill (46°53.450′N, 113°59.385′W) near Missoula, MT (Bradshaw 2004). Waterworks Hill is ∼200 m tall and has an essentially flat upwind fetch to the west of over 10 km (Fig. 3). It is covered with 8–30 cm-tall vegetation composed primarily of bunch grasses

Table 4. Mass-conserving model mesh parameters for the Waterworks Hill simulations

	Number of vertical cells	Horizontal cell size (m)	Largest aspect ratio
Grid 1	30	50	157
Grid 2	30	60	166
Grid 3	30	100	288
Grid 4	20	200	37

and forbs. Seven 3.05 m-tall temporary towers recorded 30 min average wind speed and direction. Estimated error in wind direction was $\pm 15°$ based on past experience with similar sensors. Additionally, an existing wind tower in the drainage to the east of the hill was used. This tower, called the 'Tulip Tower', also was 3.05 m tall. Data from a National Weather Service (NWS) sensor located at the Missoula Airport (elevation 975 m) ∼8 km to the west-north-west of Waterworks Hill was also used. Two-minute averaged wind speeds measured at the airport tower during a cold front passage for a period of 3 h were consistently between 9.4 m s^{-1} (10 m above ground level) and 10.3 m s^{-1} from the west. This corresponded to a Pasquill–Turner stability class D (Turner 1964), which is neutral. The domain size used was ∼21×16 km and extended 5 km above sea level (∼4000 m above ground level) with elevation data at 30-m resolution (USGS 2006) for all simulations.

Waterworks Hill mass-conserving configuration. Four simulations with differing mesh characteristics were performed for the Waterworks Hill data (Table 4). Data from a NWS surface wind sensor at the Missoula Airport were fit to a logarithmic velocity profile (Eqn 9), which was used to initialise the flow calculation. The surface roughness length (z_0) was estimated at 0.02 m based on the vegetation (Wieringa 1993). The reference velocity used in the logarithmic profile was adjusted until the simulation matched the velocity measured at the Missoula Airport NWS sensor (i.e. 9.8 m s^{-1} from 270° at a height of 10 m). The final reference velocity was 8.6 m s^{-1} from 270°, 3.05 m above the ground. All simulations used a vertical cell growth of 30%, single-point quadrature integration, and iterated to a residual tolerance of 0.1.

Waterworks Hill momentum-conserving configuration. Two simulations were conducted with different horizontal grid resolutions for the momentum-conserving model evaluations for Waterworks Hill (Table 3). Each grid had eight layers of prismatic cells adjacent to the ground and tetrahedral cells above. The cell sizes grew with height above the ground. The near wall cell height of the coarse grid was 12 m and the fine grid was 5 m. Data from the NWS tower were used to initialise the simulations with a logarithmic velocity profile.

Results and discussion

Askervein Hill: mass-conserving simulation

Simulated velocity values using the base case parameters were within 30% of the measured values everywhere, except in the lee of the hill where errors up to 150% were found (Fig. 4). At the worst location, the measured velocity was 3.2 m s^{-1} compared to a simulated value of 8 m s^{-1}. All simulated wind
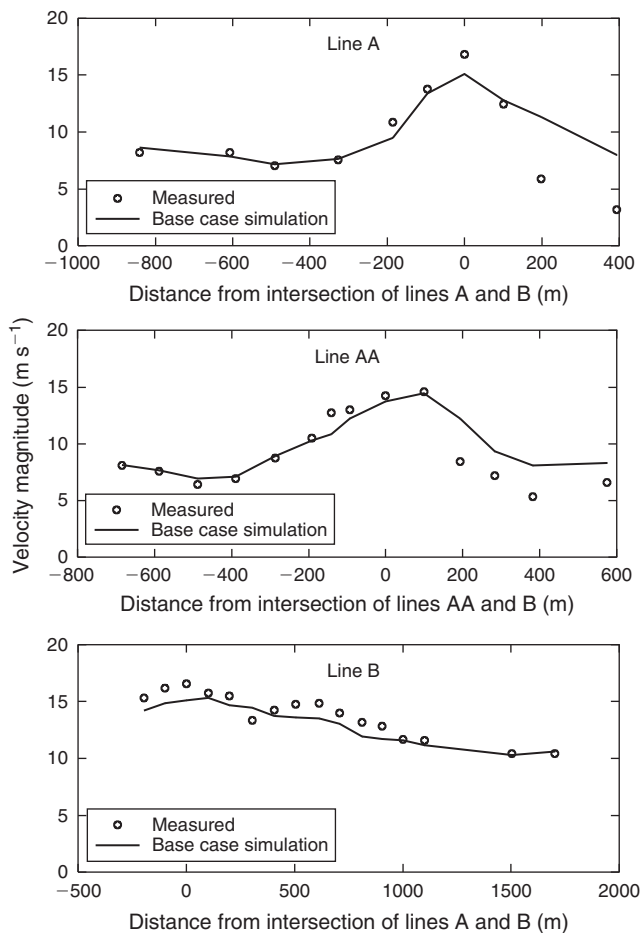
Fig. 4. Comparison of measured and simulated wind velocities using the mass-conserving model for Askervein Hill. Distances are in relation to reference lines identified in Fig. 1.

Fig. 5. Comparison of measured and simulated wind directions using the mass-conserving model for flow over Askervein Hill along line A for the base case input variable set. Distances are in relation to reference lines identified in Fig. 1.

over the hill. Users should be aware of the limitations of this model on the lee side of terrain features and use caution when interpreting the model results there. An area of future research could be to improve the model accuracy on the lee side of terrain features. An example of how this might be done is described by Brown *et al.* (2009), who used empirical parameterisation of wake flows behind buildings in a mass-conserving model to simulate flow in urban areas for emergency response.

The sensitivity to horizontal resolution and quadrature point integration accuracy was examined. Variation of the horizontal resolution over the range of 23.4–120 m does not seem to change the wind speeds, indicating that these resolutions were adequate for this terrain feature (Fig. 6*a*). Gaussian quadrature was used in the finite element simulation to perform volume integrals over the elements. The more Gauss points in the integration, the more accurate the element volume integration. No significant increase in overall simulation accuracy was obtained with 27 Gauss points compared to just one Gauss point for the base case simulation (Fig. 6*a*).

In all simulation domains, a vertically stretched grid was used such that the vertical dimension of the computational cells increased at a rate of 30% per vertical cell. A sensitivity analysis was performed on vertical resolution by varying the number of vertical cells (Fig. 6*b*). For domains with 15 and 20 layers the wind speeds were identical and gave reasonable results. As the number of layers increased to 30 and 35, accuracy decreased. The reason for the decrease in accuracy was believed to be related to cell quality issues, because as the vertical resolution is increased and the horizontal resolution stays constant, the cell aspect ratio increases. Fig. 6*c* compares two different simulations with very high cell aspect ratios and shows the trend of increasing vertical cell resolution (increasing cell aspect ratio) giving worse results. It is well documented that poor cell quality, such as very high aspect ratio, can result in poor interpolation accuracy, discretisation error and poor condition number of the global stiffness matrix in finite element solutions (Thompson *et al.* 1999) and this is likely the problem here. Based on this analysis, cell aspect ratios are recommended to be less than 400.

directions were within 22° of measured (Fig. 5) with an average error of 10.1 and the largest errors on the lee side of the hill.

The poor performance of the mass-conserving model on the lee side of the hill should not be surprising. Lopes (2003) found similar results for his mass-conserving model applied to the same data. He proposed that the error was due to the kinematic nature of the model, which we interpret as indicating the lack of any explicit accounting of the forces causing the fluid motions. A conservation of momentum equation is the standard method of accounting for these forces, and is obviously not included in our mass-conserving model. Apparently the error from excluding this in the simulation is largest on the lee side of terrain features and smaller in other areas. This may be due to the importance of an adverse pressure gradient or turbulence effects on the lee side, which may be less important on the upwind and top of the hill.

Although large errors were found on the lee side of the hill, the overall trend in wind speed (i.e. speed-up over the ridge top and reduced speeds on the lee side) was captured by the mass-conserving model. Model accuracy was best on the upstream and top of the hill. Mean flow decelerates on lee slopes due to turbulence induced by the vortices formed as the wind moves
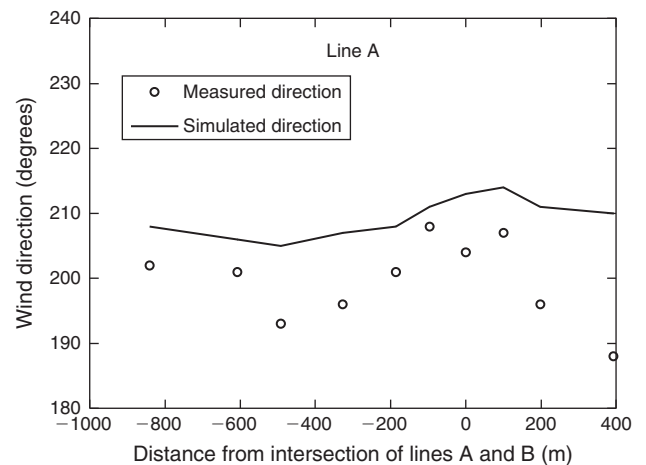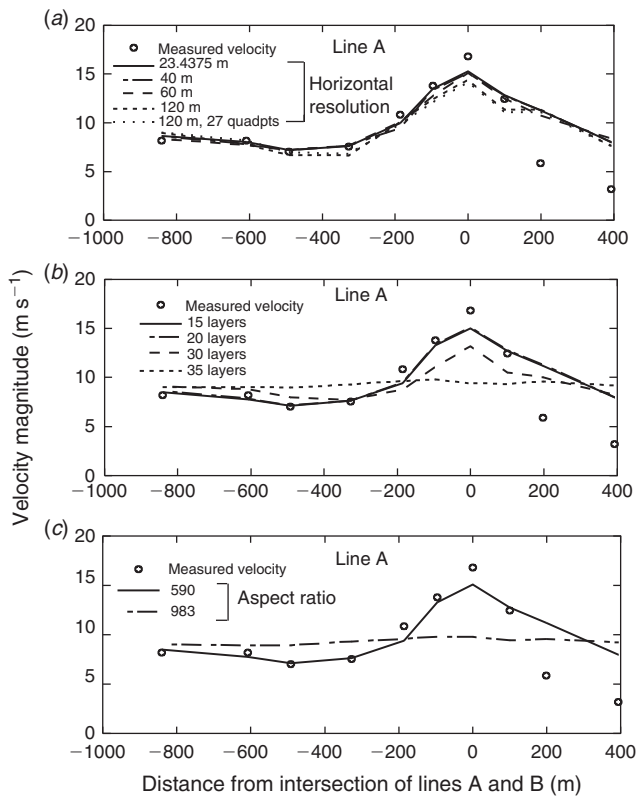
Fig. 6. Comparison of simulated *v.* measured wind velocities for mass-conserving model simulations of flow over Askervein Hill for (*a*) various horizontal cell resolutions, (*b*) various numbers of vertical cells and (*c*) two cell aspects ratios. Distances are in relation to reference lines identified in Fig. 1.

Askervein Hill: momentum-conserving simulation

Fig. 7a–c shows two momentum-conserving model simulations of different horizontal resolution compared with wind speed data. Both simulations produced wind speeds that were within 10% of the measured values except on the lee side of the hill where the errors were as high as 32%. All simulated directions were within 17° of measured (Fig. 8). The average error was 8° and the largest error occurred on the lee side of the hill. This result should be expected because this is the most difficult area to simulate due to inadequacies of the type of turbulence model used here (Kim and Boysan 1999). The increased accuracy of the speed prediction from the momentum-conserving model over the mass-conserving model on the lee side of the hill (32 *v.* 150% error for the mass-conserving model) is certainly an advantage of this model and it might be preferred if lee side flow is considered important for the particular situation.

Waterworks Hill: mass-conserving simulation

Figs 9 and 10 compare mass-conserving simulations of differing resolution with measurements from Waterworks Hill. It is evident that a mesh-insensitive solution was not reached for this site as there were differences of up to 28% between the finest grid (Grid 1) and the next finest grid (Grid 2). Unfortunately, limitations in computer memory did not allow
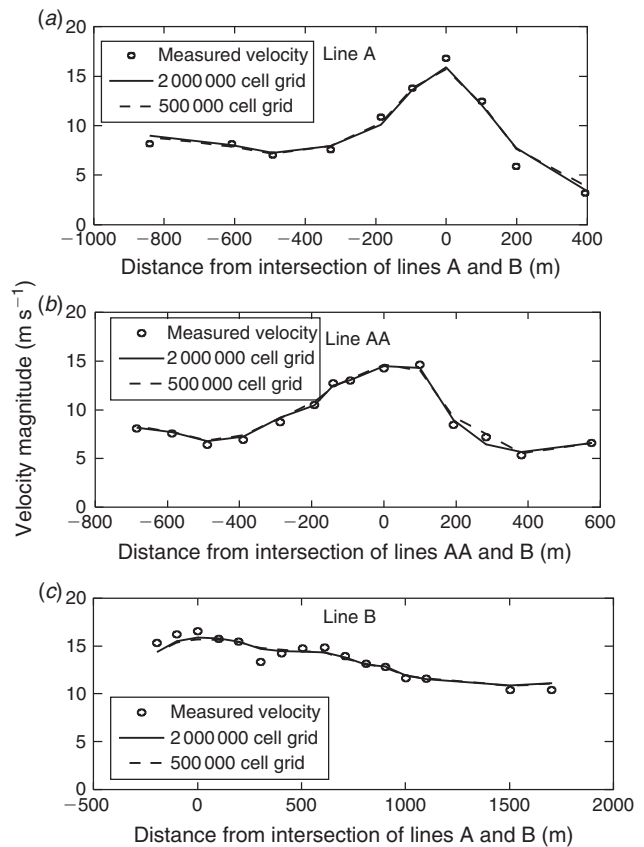

Fig. 7. Comparison of measured and simulated wind velocities from momentum-conserving model simulations of Askervein Hill. Distances are relative to measurement transects shown in Fig. 1.
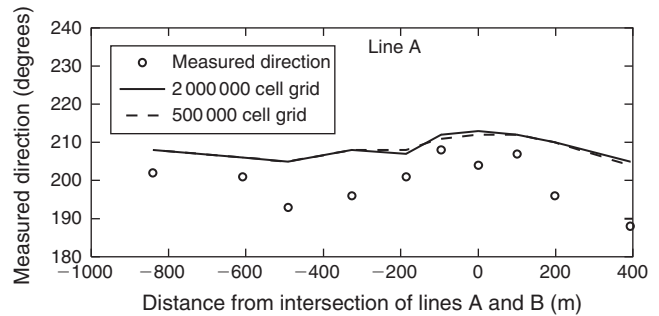

Fig. 8. Comparison of measured and simulated wind directions from momentum-conserving simulations of flow over Askervein Hill. Distances are relative to transects shown in Fig. 1.

finer grid simulations. The difference in grid independence here compared with the Askervein Hill simulations may be related to the slightly more complex topography. Apparently grid limitations are common in these types of wind simulations. Stangroom (2004) states that true grid independence is unlikely to be achieved in wind engineering problems, but that useful information is possible even from grid-dependent simulations. Lundquist *et al.* (2010) suggest the potential for grid independence with complex
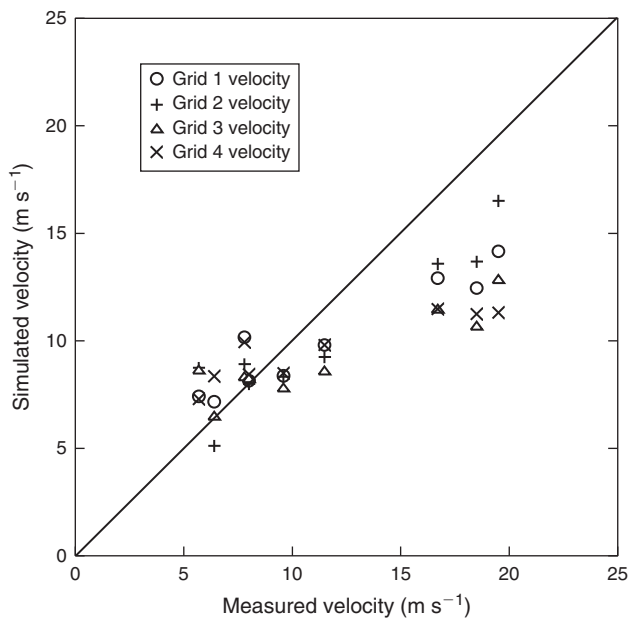
Fig. 9. Waterworks Hill results from mass-conserving model comparing simulated to measured velocity values.

Fig. 11. Comparison of measured and simulated winds for momentum-conserving model simulations of Waterworks Hill. Asterisks are measured values.
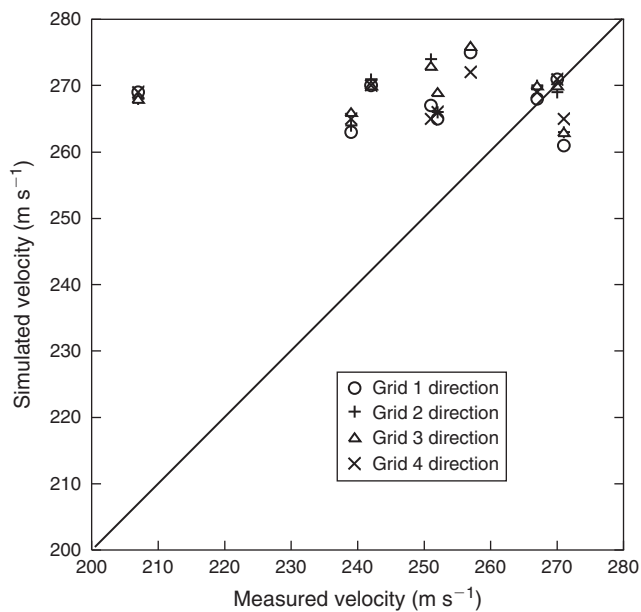

Fig. 10. Waterworks Hill results from mass-conserving model comparing simulated to measured directions.

sub-grid-scale modifications to the turbulence modelling schema.

The simulations consistently under-predicted the velocity at higher wind speed locations (generally near the top of the hill) (Fig. 9). Four possible reasons for this are hypothesised: (1) the atmosphere was not actually neutrally stable; (2) the input vertical velocity profile was incorrect (i.e. the logarithmic profile is usually only valid in the surface layer, which is ~100 m above the ground in a neutral atmosphere, but in these
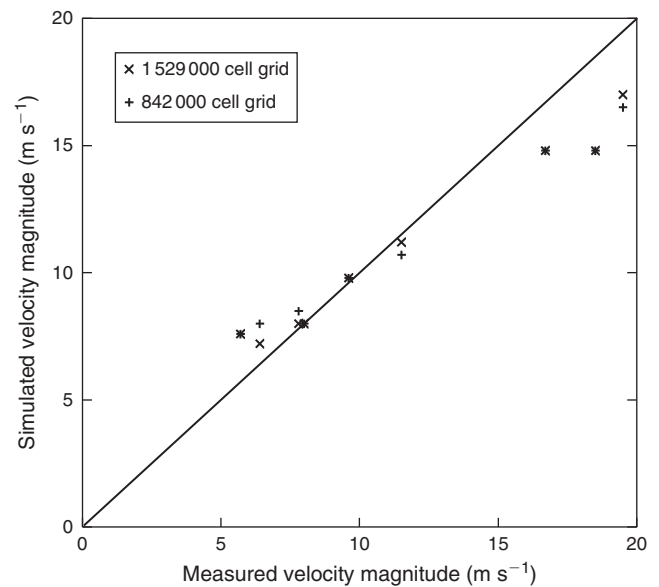
simulations it was extended to the top of the domain); (3) terrain features upwind of the Missoula Airport reference site may have disturbed the flow measured at this tower (the terrain is flat for ~10 km upwind of the tower, but further upwind a large mountain range exists); and (4) local surface roughness features, which can significantly affect the flow field near the surface, were not captured by the uniform surface roughness that was assumed for the simulations. Any of these factors could have acted separately or together to produce the under-predictions near the hill top.

All simulations over-predicted the wind speeds at the easternmost sensor point (Tulip Tower), with Grids 2 and 3 having the largest errors – 54 and 52% (Fig. 9). This tower is located at the bottom of the drainage to the east of Waterworks Hill, in an area of scattered trees and buildings. As the wind simulations assumed a uniform ground roughness value everywhere and did not account for the buildings and trees, it is unlikely that the model could have accurately simulated the Tulip Tower data. Another possibility for the over-prediction is that momentum effects on the lee of the hill produced the measured low wind speeds. Such effects are not accounted for in the model.

All simulated wind directions were within 28° of the measured values, except for one location where the largest difference was 62° (Fig. 10). This was at the most southern station shown in Fig. 3. It is not obvious why such a large discrepancy occurred here, and one possibility is that the sensor was not correctly oriented towards north when placed. Predicted wind direction of the other stations was on the order of one to two times the estimated uncertainty in the measured wind directions (i.e. ±15°).

Waterworks Hill: momentum-conserving simulation

The two mesh resolutions produced similar results for wind speed (Fig. 11). Both the coarse and fine simulations
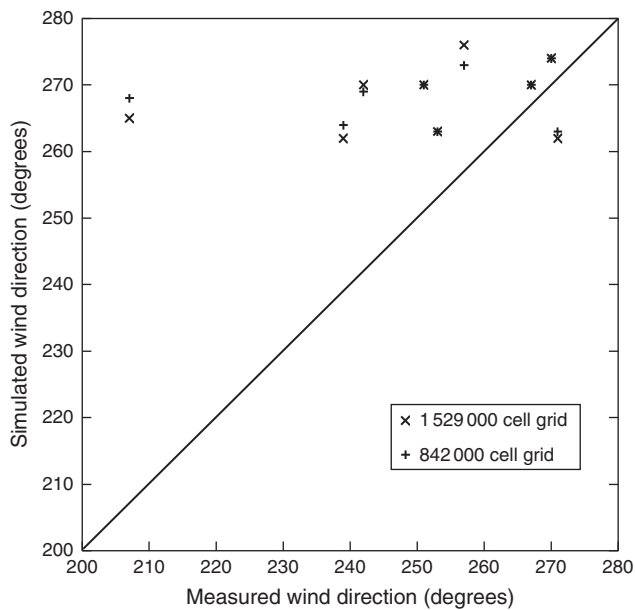
Fig. 12. Comparison of measured and simulated wind directions for momentum-conserving simulations of Waterworks Hill. Asterisks are measured values.

under-predicted the speeds at the higher elevation towers. Reasons for this under-prediction may be the same as hypothesised for the mass-conserving model simulations. The largest error of 33.9% occurred at the eastern most station (Tulip Tower), as in the mass-conserving simulations. Again, roughness effects may have affected measurements here. Also, as was shown in the Askervein simulations, the comparison suggests that lee side locations are the most difficult to predict, again likely because of turbulence model deficiencies.

The fine and coarse grids produced wind directions that were within 28° of the measured values for all locations but one, the southernmost station, where the simulated winds were 61° greater than measured (Fig. 12). As mentioned before, this station may have been oriented incorrectly when placed.

Mass-conserving v. momentum-conserving results

Both models performed reasonably well on the upwind side and top of the terrain features investigated. Reduced accuracy was observed in both models on the lee sides, although the momentum-conserving model performed better than the mass-conserving model. This difference is due to a more complete handling of momentum and turbulence in the model equations. Fire managers simulating wind where lee side areas are important should be aware of the limitations of the models here and the differences in model capabilities.

Lopes (2003) also investigated both a momentum-conserving model and a mass-conserving model and reported that on the lee side of Askervein Hill, the momentum-conserving model more closely matched measurements. However, in his other simulations of more complex terrain, the momentum-conserving results did not show any improvement over the mass-conserving model. This was attributed to a poor description of the approach flow compared to the Askervein Hill data, and possibly inaccurate characterisation of location terrain features and surface

roughness in the complex terrain simulations. Chow and Street (2009) reached the same conclusion using a state-of-the-art, high-order, sub-grid-scale turbulence model. In some applications, such as support of wildland fire management, the approach flow may not be known very accurately, which could negate the apparent increased accuracy of a momentum-conserving model. Further model comparisons in more complex terrain (greater elevation differences, steeper slopes, multiple adjacent terrain features) would give better insight into this issue. The mass-conserving model computes wind fields in seconds to a few minutes, whereas the momentum-conserving model takes 30 to 90 min per simulation on typical laptop computers using one CPU (2 GHz, 3 GB RAM).

Overall, there appears to be a clockwise bias to the direction predictions for both models across the two datasets. One possibility for this bias is that terrain features upstream of the measurement location and outside of the simulation domain generated consistent downstream flow characteristics that were not captured by the modelling approach taken here. Regardless, it is difficult to reach any conclusion without further comparison against additional datasets, of which few if any exist.

Conclusions

The mathematical foundations of two diagnostic models for predicting surface wind flow at very high spatial resolutions were presented and model-simulated surface winds were compared against two field datasets collected from low elevation hills.

Simulated speeds from the momentum-conserving model were within 32 and 10% of measured values on the lee and windward sides of the terrain features. The results suggest that the model is most accurate in simulating upslope and hill crest flow. Clearly, such models could be very useful for simulating wind flow in complex terrain in support of wildland fire management. Further case studies in terrain of higher complexity would be useful in determining the model accuracy.

The mass-conserving model produced wind speeds within 30% of measured values for locations other than the lee side of terrain obstructions, where errors reached 150%. The increased error on the lee side of terrain obstacles was most likely due to the model not explicitly incorporating a momentum equation. Simulations in steeper, more rugged terrain would be expected to give less accurate results. Ultimately, 'acceptable accuracy' must be determined by the user and will depend on the specific application. However, as also concluded by Lopes (2003), numerical tools such as the two described here should at least give fire managers information on the relative wind characteristics associated with different terrain locations.

As fire management decision time frames are short and simulation times for the momentum-conserving model are ~60 times slower, the mass-conserving model may be more useful and practical. The trade-off may be loss of some accuracy, especially in the wake region of a terrain feature. In some cases it may be impossible to quantify the approach flow sufficiently to improve accuracy over a mass-conserving modelling approach by incorporation of a momentum solution. Mass-conserving model predictions could likely be improved without sacrificing computational requirements if available meso-scale forecast

data were used for initialisation. Such a combination could account for both the meso-scale meteorology and the local terrain effects (Petersen *et al.* 1997; Beaucage *et al.* 2014).

The analysis presented here assumes steady-state conditions and neutral stability, and was performed on what can be characterised as gently rolling terrain. The results suggest that either surface wind modelling method could contribute to improved accuracy in wildland fire management decisions using minimal computing resources, little advanced training and short simulation time.

Future work will include evaluations for different types of complex terrain features under a range of metrological conditions, further exploration of the dependence of simulation accuracy on mesh resolution and evaluation of the utility of these models for dynamically downscaling winds from meso-scale weather models (N. S. Wagenbrenner, B. K. Lamb, J. M. Forthofer, K. S. Shannon and B. W. Butler, unpubl. data).

Acknowledgements

References

Ager A, Finney M, McMahan A, Cathcart J (2010) Measuring the effect of fuel treatments on forest carbon using landscape risk analysis. *Natural Hazards and Earth System Sciences* **10**, 2515–2526. doi:10.5194/NHESS-10-2515-2010

Albini FA (1982) Response of free-burning fires to nonsteady wind. *Combustion Science and Technology* **29**, 225–241. doi:10.1080/00102208208923599

Alm LK, Nygaard TA (1995) Flow over complex terrain estimated by a general purpose Navier–Stokes solver. *Modelling, Identification and Control* **16**, 169–176. doi:10.4173/MIC.1995.3.5

Apsley DD, Castro IP (1997) Flow and dispersion over hills: comparison between numerical predictions and experimental data. *Journal of Wind Engineering and Industrial Aerodynamics* **67–68**, 375–386. doi:10.1016/S0167-6105(97)00087-1

Atkinson BW (1995) Introduction to the fluid mechanics of meso-scale flow fields. In 'Diffusion and Transport of Pollutants in Atmospheric Meso-scale Flow Fields'. (Ed. A Gyr, F-S Rys) Vol. 1, pp. 1–20. (Kluwer: Dordrecht, the Netherlands)

Barnard JC (1991) An evaluation of three models designed for siting wind turbines in areas of complex terrain. *Solar Energy* **46**, 283–294. doi:10.1016/0038-092X(91)90096-F

Barrett R, Berry M, Chan TF, Demmel J, Donato J, Dongarra J, Eijkhout V, Pozo R, Romine C (1994) 'Templates for the Solution of Linear Systems: Building Blocks for Iterative Methods', 2nd edn. (SIAM: Philadelphia, PA)

Beaucage P, Brower MC, Tensen J (2014) Evaluation of four numerical wind flow models for wind resource mapping. *Wind Energy* **17**, 197–208. doi:10.1002/WE.1568

Boussinesq J (1877) Théorie de l'Écoulement Tourbillant. *Memoires présentés par divers savant à l'Académie des Sciences de l'Institut de France* **23**, 46–50.

Bradshaw L (2004) Wind measurements over Waterworks Hill, Missoula, MT. USDA Forest Service, Rocky Mountain Research Station, Missoula Fire Science Laboratory, Internal Report. (Missoula, MT)

Brown M, Gowardhan A, Nelson M, Williams M, Pardyjak E (2009) Evaluation of the QUIC wind and dispersion models using the Joint Urban 2003 Field Experiment. In 'Proceedings of the Eighth Symposium on the Urban Environment', 10–15 January 2009, Phoenix AZ. (Eds PM Klein, AJ Brazel, JK Lundquist, J Davis) paper 19.4. (American Meteorological Society) Available at https://ams.confex.com/ams/pdfpapers/146140.pdf [Verified 5 August 2014]

Butler BW, Bartlette RA, Bradshaw LS, Cohen JD, Andrews PL, Putnam T, Mangan RJ (1998) Fire behavior associated with the 1994 south canyon fire on storm king mountain, Colorado. USDA Forest Service, Rocky Mountain Research Station, Research Paper RMRS-RP-9. (Fort Collins, CO)

Byram GM, Nelson RM (1974) Bouyancy characteristics of a fire heat source. *Fire Technology* **10**, 68–79. doi:10.1007/BF02590513

Castro FA, Palma JMLM, Silva Lopes A (2003) Simulation of the Askervein Flow. Part1: Reynolds averaged Navier–Stokes equations (k-epsilon turbulence model). *Boundary-Layer Meteorology* **107**, 501–530. doi:10.1023/A:1022818327584

Catchpole WR, Catchpole EA, Butler BW, Rothermel RC, Morris GA, Latham DJ (1998) Rate of spread of free-burning fires in woody fuels in a wind tunnel. *Combustion Science and Technology* **131**, 1–37. doi:10.1080/00102209808935753

Chan ST, Sugiyama G (1997) User's manual for MC_WIND: A new mass-consistent wind model for ARAC-3. Lawrence Livermore National Laboratory, UCRL-MA-129067. (Oak Ridge, TN)

Chow FK, Street RL (2009) Evaluation of turbulence closure models for large-eddy simulation over complex terrain: flow over Askervein Hill. *Journal of Applied Meteorology and Climatology* **48**, 1050–1065. doi:10.1175/2008JAMC1862.1

Clark TL, Coen J, Latham D (2004) Description of a coupled atmosphere-fire model. *International Journal of Wildland Fire* **13**, 49–63. doi:10.1071/WF03043

Coen JL, Cameron M, Michalakes J, Patton EG, Riggan PJ, Yedinak KM (2013) WRF-Fire: coupled weather–wildland fire modeling with the weather research and forecasting model. *Journal of Applied Meteorology and Climatology* **52**, 16–38. doi:10.1175/JAMC-D-12-023.1

Davis CG, Bunker SS, Mutschlecner JP (1984) Atmospheric transport models for complex terrain. *Journal of Climate and Applied Meteorology* **23**, 235–238. doi:10.1175/1520-0450(1984)023<0235:ATMFCT>2.0.CO;2

Finardi S, Brusasca G, Morselli MG, Trombetti F, Tampieri F (1993) Boundary-layer flow over analytical two-dimensional hills: a systematic comparison of different models with wind tunnel data. *Boundary-Layer Meteorology* **63**, 259–291. doi:10.1007/BF00710462

Finney MA (1998) FARSITE: Fire area simulator-model development and evaluation. USDA Forest Service, Rocky Mountain Research Station, Research Paper RMRS-RP-4. (Ogden, UT)

Finney M, Grenfell IC, McHugh C, Seli R, Trethewey DL, Stratton RD, Brittain S (2011) A method for ensemble wildland fire simulation. *Environmental Modeling and Assessment* **16**, 153–167. doi:10.1007/S10666-010-9241-3

Forthofer JM (2007) Modeling wind in complex terrain for use in fire spread prediction. MSc thesis, Colorado State University, Fort Collins.

Forthofer JM, Butler BW, McHugh C, Finney MA, Bradshaw LS, Stratton R, Shannon KS, Wagenbrenner NS (2014) A comparison of three approaches for simulating fine-scale surface winds in support of wildland fire management. Part II. An exploratory study of the impact of simulated winds on fire growth simulations. *International Journal of Wildland Fire*. [Published online early 18 August 2014] doi:10.1071/WF12089

Geai P (1987) Methode d'interpolation et de reconstitution tridimensionelle d'un champ de vent: le code d'analyse objective MINERVE. Report DER/HE/34–87.03E.d.F. (Chatou, France)

Homicz GF (2002) Three-dimensional wind field modeling: a review. Sandia National Laboratories, SAND Report 2597. (Albuquerque, NM)

Jackson PS, Hunt JCR (1975) Turbulent wind flow over a low hill. *Quarterly Journal of the Royal Meteorological Society* **101**, 929–955. doi:10.1002/QJ.49710143015

Kim S-E, Boysan F (1999) Application of CFD to environmental flows. *Journal of Wind Engineering and Industrial Aerodynamics* **81**, 145–158. doi:10.1016/S0167-6105(99)00013-6

Kim HG, Patel VC, Lee CM (2000) Numerical simulation of wind flow over hilly terrain. *Journal of Wind Engineering and Industrial Aerodynamics* **87**, 45–60. doi:10.1016/S0167-6105(00)00014-3

Kochanski AK, Jenkins MA, Mandel J, Beezley JD, Krueger SK (2013) Real time simulation of 2007 Santa Ana fires. *Forest Ecology and Management* **294**, 136–149. doi:10.1016/J.FORECO.2012.12.014

Linn RR, Reisner J, Colman JJ, Winterkamp J (2002) Studying wildfire behavior using FIRETEC. *International Journal of Wildland Fire* **11**, 233–246. doi:10.1071/WF02007

Lopes AMG (2003) WindStation – a software for the simulation of atmospheric flows over complex topography. *Environmental Modelling & Software* **18**, 81–96. doi:10.1016/S1364-8152(02)00024-5

Lundquist JD, Minder JR, Neiman PJ, Sukovich E (2010) Relationships between barrier jet heights, orographic precipitation gradients, and streamflow in the Northern Sierra Nevada. *Journal of Hydrometeorology* **11**, 1141–1156. doi:10.1175/2010JHM1264.1

Mason PJ, King JC (1985) Measurements and predictions of flow and turbulence over an isolated hill of moderate slope. *Quarterly Journal of the Royal Meteorological Society* **111**, 617–640. doi:10.1002/QJ.49711146818

Maurizi A, Palma JMLM, Castro FA (1998) Numerical simulation of the atmospheric flow in a mountainous region of the north of Portugal. *Journal of Wind Engineering and Industrial Aerodynamics* **74–76**, 219–228. doi:10.1016/S0167-6105(98)00019-1

Mell WE, Jenkins MJ, Gould JS, Cheney NP (2007) A physics-based approach to modelling grassland fires. *International Journal of Wildland Fire* **16**, 1–22. doi:10.1071/WF06002

Mellor GL, Yamada T (1982) Development of a turbulence closure model for geophysical fluid problems. *Reviews of Geophysics* **20**, 851–875. doi:10.1029/RG020I004P00851

Montavon C (1998) Validation of a non-hydrostatic numerical model to simulate stratified wind fields over complex topography. *Journal of Wind Engineering and Industrial Aerodynamics* **74–75**, 1762–1782.

Montero G, Montenegro R, Escobar JM (1998) A 3-D diagnostic model for wind field adjustment. *Journal of Wind Engineering and Industrial Aerodynamics* **74–76**, 249–261. doi:10.1016/S0167-6105(98)00022-1

Mortensen NG, Landberg L, Troen I, Petersen EL (1993) Wind atlas analysis and application program (WAsP). Vol. 2: User's guide. Riso National Laboratory. (Roskilde, Denmark)

Moussiopoulos N, Flassak T (1986) Two vectorized algorithms for the effective calculations of mass-consistent flow fields. *Journal of Applied Meteorology* **25**, 847–857. doi:10.1175/1520-0450(1986)025<0847:TVAFTE>2.0.CO;2

Parkinson HG (1987) Measurements of wind flow over models of a hill. PhD thesis, University of Oxford, Trinity.

Petersen EL, Mortensen NG, Landberg L, Hojstrup J, Frank HP (1997) Wind power meteorology. Riso National Laboratory, Wind Energy Department Riso-I-1206(EN). (Roskilde, Denmark)

Raithby GD, Stubley GD, Taylor PA (1987) The Askervein Hill Project: a finite control volume prediction of three-dimensional flows over the hill. *Boundary-Layer Meteorology* **39**, 247–267. doi:10.1007/BF00116121

Richards P, Hoxey R (1993) Appropriate boundary conditions for computational wind engineering models using the k-epsilon turbulence model. *Journal of Wind Engineering and Industrial Aerodynamics* **46–47**, 145–153. doi:10.1016/0167-6105(93)90124-7

Rodi W (1997) Comparison of LES and RANS calculations of the flow around bluff bodies. *Journal of Wind Engineering and Industrial Aerodynamics* **69–71**, 55–75. doi:10.1016/S0167-6105(97)00147-5

Ross DG, Smith IN, Manins PC, Fox DG (1988) Diagnostic wind field modeling for complex terrain: model development and testing. *Journal of Applied Meteorology* **27**, 785–796. doi:10.1175/1520-0450(1988)027<0785:DWFMFC>2.0.CO;2

Rothermel RC (1972) A mathematical model for predicting fire spread in wildland fuels. USDA Forest Service, Intermountain Research Station, Research Paper INT-115. (Ogden, UT)

Rothermel RC (1993) Mann Gulch fire: a race that couldn't be won. USDA Forest Service, Intermountain Research Station, General Technical Report INT-299. (Ogden, UT)

Sasaki Y (1958) An objective analysis based on the variational method. *Journal of the Meteorological Society of Japan* **36**, 77–88.

Sasaki Y (1970*a*) Numerical variational analysis formulated under the constraints determined by longwave equations and low-pass filter. *Monthly Weather Review* **98**, 884–898. doi:10.1175/1520-0493(1970)098<0884:NVAFUT>2.3.CO;2

Sasaki Y (1970*b*) Some basic formalisms in numerical variational analysis. *Monthly Weather Review* **98**, 875–883. doi:10.1175/1520-0493(1970)098<0875:SBFINV>2.3.CO;2

Scire JS, Robe FR, Fernau ME, Yamartino RJ (2000) 'A User's Guide for the CALMET Meteorological Model.' (Earth Tech, Inc.: Concord, MA)

Sherman CA (1978) A mass-consistent model for wind fields over complex terrain. *Journal of Applied Meteorology* **17**, 312–319. doi:10.1175/1520-0450(1978)017<0312:AMCMFW>2.0.CO;2

Stangroom P (2004) CFD modeling of wind flow over terrain. PhD thesis, The University of Nottingham.

Stratton RD (2006) Guidance on spatial wildland fire analysis: models, tools, and techniques. USDA Forest Service, Rocky Mountain Research Station, General Technical Report RMRS-GTR 183. (Fort Collins, CO)

Sun R, Krueger SK, Jenkins MA, Zulauf MA, Charney JJ (2009) The importance of fire–atmosphere coupling and boundary-layer turbulence to wildfire spread. *International Journal of Wildland Fire* **18**, 50–60. doi:10.1071/WF07072

Taylor PA, Teunissen HW (1983) Askervein '82: report on the September/October 1982 Experiment to study boundary layer flow over Askervein, South Uist. Atmospheric Environment Service, MSRB-83-8. (Downsview, ON)

Taylor PA, Teunissen HW (1985) The Askervein Hill Project: report on the September/October 1983 Main Field Experiment. Atmospheric Environment Service, MSRB-84-6. (Downsview, ON)

Taylor PA, Teunissen HW (1987) The Askervein Hill Project: overview and background data. *Boundary-Layer Meteorology* **39**, 15–39. doi:10.1007/BF00121863

Thompson EG (2005) 'Introduction to the Finite Element Method: Theory, Programming, and Applications.' (Wiley: Hoboken, NJ)

Thompson JF, Soni BK, Weatherill NP (1999) 'Handbook of Grid Generations.' (CRC Press: Boca Raton, FL)

Turner DB (1964) A diffusion model for an urban area. *Journal of Applied Meteorology* **3**, 83–91. doi:10.1175/1520-0450(1964)003<0083:ADMFAU>2.0.CO;2

Uchida T, Ohya Y (1999) Numerical simulation of atmospheric flow over complex terrain. *Journal of Wind Engineering and Industrial Aerodynamics* **81**, 283–293. doi:10.1016/S0167-6105(99)00024-0

Undheim O, Andersson HI, Berge E (2006) Non-linear, microscale modelling of the flow over Askervein Hill. *Boundary-Layer Meteorology* **120**, 477–495. doi:10.1007/S10546-006-9065-5

USDA Forest Service and USDI Bureau of Land Management (2002) Price Canyon Fire Entrapment Investigation Report. (Missoula, MT) Available at https://www.iaff.org/hs/LODD_Manual/LODD%20Reports/

South%20Canyon,%20CO%20-%2014%20LODDs.pdf [Verified 26 June 2014]

USGS (2006) Fire data ordering system. Available at http://firedata.cr.usgs.gov [Verified 26 June 2014].

Vandoormaal JP, Raithby GD (1984) Enhancements of the SIMPLE method for predicting incompressible fluid flows. *Numerical Heat Transfer Part A* **7**, 147–163.

Walmsley JL, Taylor PA (1996) Boundary-layer flow over topography: impacts of the Askervein Study. *Boundary-Layer Meteorology* **78**, 291–320. doi:10.1007/BF00120939

Walmsley JL, Taylor PA, Keith T (1986) A simple model of neutrally stratified boundary layer flow over complex terrain with surface roughness modulations (MS3DJH/3R). *Boundary-Layer Meteorology* **36**, 157–186. doi:10.1007/BF00117466

Walmsley JL, Troen IB, Demetrius P, Lalas DP, Mason PJ (1990) Surface-layer flow in complex terrain: comparison of models and full-scale observations. *Boundary-Layer Meteorology* **52**, 259–281. doi:10.1007/BF00122090

Wieringa J (1993) Representative roughness parameters for homogenous terrain. *Boundary-Layer Meteorology* **63**, 323–363. doi:10.1007/BF00705357

Yakhot V, Orszag SA (1986) Renormalization group analysis of turbulence. I. Basic theory. *Journal of Scientific Computations* **1**, 3–51. doi:10.1007/BF01061452